ADVANCED THERAPEUTICS
www.advtherap.com

Intratumoral Nanofluidic System for Enhancing Tumor Biodistribution of Agonist CD40 Antibody

*Corrine Ying Xuan Chua, Jeremy Ho, Antonia Susnjar, Graziano Lolli, Nicola Di Trani, Federica Pesaresi, Mengying Zhang, Elizabeth Nance, and Alessandro Grattoni**

Tumor uptake and biodistribution of immunotherapy is associated with clinical response as well as toxicity. To augment immunotherapy bioavailability in the tumor, an intratumoral administration route via direct injection or local release technologies has emerged as an appealing approach. Here the biodistribution of an agonistic anti-CD40 monocolonal antibody (CD40 mAb) when sustainably delivered via an intratumoral nanofluidic drug-eluting seed (NDES) is evaluated in comparison to systemic or direct intratumoral administration. The NDES achieves sustained drug release through diffusion by leveraging electrostatic nanoconfinement within nanochannels, without requiring internal or external actuation. Using the 4T1 murine mammary carcinoma model, the biodistribution of Alexa Fluor-700 conjugated CD40 mAb is tracked via fluorescence imaging analysis, comparing three routes of administration over 7 and 14 days. NDES-treated cohort shows sustained high levels of intratumoral CD40 mAb without off-target organ exposure, compared to the intraperitoneal and direct intratumoral administration. Moreover, radiation pre-treatment of the 4T1 tumors augments tumor retention of CD40 mAb in the NDES group. Overall, sustained intratumoral release of CD40 mAb via the NDES improves local drug bioavailability without systemic dissemination, suggesting an enhanced approach for immunotherapy administration.

1. Introduction

While immunotherapy has emerged as a pillar of cancer treatment in recent years, only a fraction of patients respond. Poor drug distribution and tumor uptake are often overlooked as mechanisms of resistance to treatment.[1] A recent clinical study assessing atezolizumab biodistribution revealed that high tumor uptake correlated to treatment response.[2] Along this line, other clinical findings showed improved disease states in cancer patients with reduced clearance of nivolumab or durvalumab.[3–5] Beyond the variabity in response rate, another concern of immunotherapy is accumulation in off-target organs, leading to treatment-limiting toxicities.[6–8] The clinical correlation of tumor uptake and response as well as toxicity due to off-target organ biodistribution is currently under further investigation in a clinical trial with ipilimumab (NCT03313323). Considering these factors, a better understanding of the pharmacokinetic and biodistribution properties of immunotherapeutic

Dr. C. Y. X. Chua, Dr. J. Ho, A. Susnjar, G. Lolli, N. Di Trani, F. Pesaresi, Dr. A. Grattoni
Department of Nanomedicine
Houston Methodist Research Institute
Houston, TX 77030, USA
E-mail: agrattoni@houstonmethodist.org
Dr. J. Ho
Weill Cornell Medical College
New York, NY 10065, USA
G. Lolli
Department of Mechanical and Aerospace Engineering
Polytechnic of Turin
Turin 10129, Italy
N. Di Trani
University of Chinese Academy of Science (UCAS)
Shijingshan, 19 Yuquan Road Beijing 100049, China
F. Pesaresi
Department of Electronics and Telecommunications
Polytechnic of Turin
Turin 10129, Italy
M. Zhang, Dr. E. Nance
Department of Chemical Engineering
University of Washington
Seattle, WA 98195, USA
Dr. A. Grattoni
Department of Surgery
Houston Methodist Hospital
Houston, TX 77030, USA
Dr. A. Grattoni
Department of Radiation Oncology
Houston Methodist Hospital
Houston, TX 77030, USA

The ORCID identification number(s) for the author(s) of this article can be found under https://doi.org/10.1002/adtp.202000055

DOI: 10.1002/adtp.202000055

antibodies are warranted to refine dosing strategies for enhancing therapeutic index.

Local drug administration is purported to maximize tumor concentration while minimizing systemic exposure, and hence reduce side effects.[9] By confining immunotherapy locally, the tumor is leveraged as an in-situ vaccine, priming a polyclonal immune response against tumor antigens to induce durable antitumor immunity.[10,11] This paradigm is increasingly investigated in clinical trials.[10–12] Of relevance, CD40, a member of the tumor necrosis factor receptor superfamily, is an appealing candidate for local immunostimulatory immunotherapy.[10] Agonistic anti-CD40 monocolonal antibodies (CD40 mAb) provide a stimulus for immune recognition of tumor antigens through dendritic cells and consequently, the priming of a robust T cell response.[13] While CD40 mAb has demonstrated efficacy, systemic administration limits clinical use due to toxicities such as cytokine release syndrome and hepatotoxicity.[14–18] On the basis of numerous promising preclinical studies,[14,19–22] local CD40 mAb administration via direct intratumoral injection is actively explored in phase I clinical trials (NCT03892525, NCT02379741, NCT03329950). However, as substantiated in a recently published report, intratumoral bolus injection does not ensure elimination of collateral toxicity.[23] Repeated injections of ADC-1013, an agonistic anti-CD40 mAb at a low dose (approximately 3-fold lower than systemic), provoked adverse effects in 83% of patients, with 27% of those of grade 3 or 4.[23] Adverse events were related to cytokine release, plausibly attributable to rapid leakage of ADC-1013 into the systemic circulation. Further, intratumoral fluid injections of therapeutics are linked to fast drug elimination due to the increased tumor interstitial fluid pressure.[24]

On this note, sustained release local delivery platforms have emerged as a potential solution for obviating repeated intratumoral injections.[9,25] Through controlled released mechanisms, a small dose is locally delivered in a sustained manner over a predefined duration. Our group and others have demonstrated that sustained local release of CD40 mAb has antitumor efficacy with reduced systemic toxicity.[14,19–22,26,27] Specifically, using our intratumoral nanofluidic drug-eluting seed (NDES), we demonstrated antitumor response with concomitant reduction in hepatoxicity in the 4T1 murine model of triple negative breast cancer (TNBC).[27] However, as intratumoral delivery is beginning to make headway in the clinic, optimal dosing strategies need to be elucidated. Thus far, evaluation of pharmacokinetic properties and biodistribution of locally injected CD40 mAb, which could inform on dosing regimen, are limited to a short duration of up to 72 h after administration.[22] Little is known about long term biodistribution and tumor bioavailability of immunotherapeutics, which is of particular interest when considering the increasing clinical appeal of sustained release local delivery systems for cancer treatment.[25]

In this study, we sought to demonstrate the effects of sustained local release of CD40 mAb on pharmacokinetics, intratumoral bioavailability, and tissue biodistribution. By tracking fluorescently labelled CD40 mAb, we compared sustained release via NDES to systemic and bolus intratumoral routes of administration in the 4T1 triple negative breast cancer mouse model. Consistent with our hypothesis, both intratumoral injection and NDES reduced systemic biodistribution compared to intraperitoneal administration. Specifically, we demonstrated that sustained intratumoral release of CD40 mAb via NDES increased local bioavailability with minimal systemic dissemination. Further, due to clinical evidence of synergy between immunotherapy and radiation treatment[28] including that of CD40 mAb,[29–31] we investigated the impact of hypofractionated radiotherapy on mAb pharmacokinetics and biodistribution. The addition of hypofractionated radiotherapy increased intratumoral bioavailability of CD40 mAb when administered intratumorally via the NDES. Overall, we demonstrated that sustained intratumoral release of CD40 mAb via the NDES is a viable approach for maintaining drug locally without systemic dissemination.

2. Results

2.1. NDES Device

The NDES is an intratumorally implanted platform for controlled release of anticancer therapeutics (**Figure 1**A).[27,32] Intratumoral implantation is performed using a trocar approach, similar to clinical insertion of brachytherapy seeds. Sustained release from the NDES is achieved intratumorally (Figure 1B) via a silicon nanofluidic membrane[33] affixed on the drug reservoir (Figures 1C,D). The nanofluidic membrane contains 4 deep-silicon etched macrochannels (Figure 1D), each with an internal array of interconnected microchannels and slit-nanochannels (Figure 1C). Drug release through the membrane is regulated by nanoconfinement, whereby molecules diffusing through the nanochannels are exposed to electrostatic and steric interactions within the channel walls.[34–36] Thus, a saturated diffusive transport largely dependent on concentration gradient is achieved, yielding constant and sustained molecular release kinetics. In other words, the concentration difference between the reservoir and tumor drives diffusion of antibody from the NDES into the surrounding microenvironment. As such, no power sources, actuation, or physical manipulation are required for drug release upon intratumoral implantation. Given the release kinetics of the NDES, the amount of payload per unit of time is constant and sustained, until nearing drug depletion. Drug release rate is controlled by the dimension and quantity of nanochannels. Based on our previous analysis of CD40 release from the NDES,[27] nanochannel size of 20 and 250 nm were chosen for this study. Considering the nanochannel size and sustained delivery mechanism, the payload is thus shielded from immune response prior to release.

To quantify the release rate of CD40 from the NDES, in vitro release of CD40 using nanochannel sizes of 20 and 250 nm over 21 days were analyzed. Cumulative release results obtained for 20 nm NDES in our previous work were analyzed to obtain release rates.[27] With 20 nm membrane, release rate of CD40 was 3.0 ± 1.2 μg day^{-1} (mean ± standard deviation; STD), with a median of 3.1 μg day^{-1} (interquartile range (IQR), 2.5 to 4.1 μg day^{-1}) (Figure 1E). As for the 250 nm membrane, mean release rate of 6.4 ± 1.5 μg day^{-1} (median of 6.8 μg day^{-1} (interquartile range (IQR), 5.0 to 7.4 μg day^{-1}) was achieved, corresponding to a ≈2.1-fold increase.

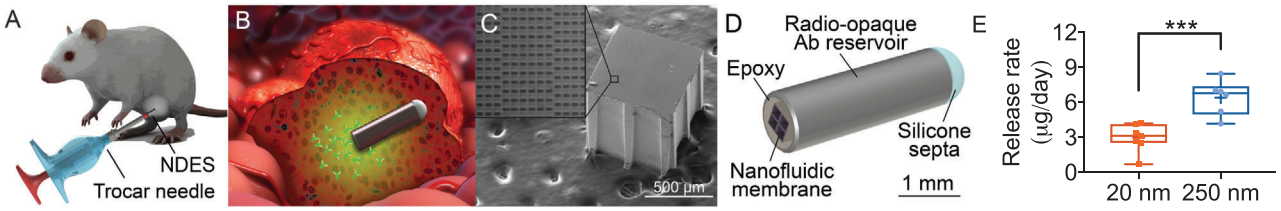

Figure 1. Sustained intratumoral drug release via nanofluidic drug-eluting seed (NDES). A) The NDES is intratumorally implanted using a minimally-invasive trocar approach. B) Upon intratumoral implantation, sustained intratumoral immunotherapeutic antibody elution occurs, regulated by a silicon nanofluidic membrane (backgroung 3D-rendering aquired from shutterstock.com) C) Scanning electron microscopy (SEM) image shows silicon nanofluidic membrane with microchannels (inset). Scale bar represents 500 μm. D) Rendering of NDES depicting nanofluidic membrane mounted on a radio-opaque stainless steel drug reservoir with epoxy. The other extremity of the reservoir is sealed with self-sealing silicone. E) Release rate of CD40 from the NDES. NDES with either 20 nm ($n = 7$) or 250 nm ($n = 6$) nanochannel membranes were used for release rate quantification over 21 days in a sink solution of 1X PBS at 37 °C. Data for 20 nm membranes was obtained through analysis of cumulative release results previously published by this group.[27] Box plot shows median, mean ("+"), interquartile ranges (25th and 75th percentiles), and all data points. Statistical significance was determined via unpaired t test. *$p < 0.05$.

2.2. NDES Release of AF700-CD40 is Sustained Intratumorally

We covalently conjugated CD40 mAb with Alexa Fluor 700 (AF700) fluorescent dye to track and visualize drug biodistribution in vivo. We selected AF700 due to its red/near-infrared excitation and emission spectra, which are minimally attenuated by tissues such as the skin and fur. Further, AF700 conjugation to CD40 mAb allows for stable, trackable fluorescent signal in vivo, obviating the need for radioactive exposure associated with radioisotope labeling.

To evaluate AF700-CD40 tumor distribution, we used the 4T1 orthotopic and syngeneic murine TNBC as our model. 4T1 tumors are visibly protruded (Figure S1A, Supporting Information), hence enabling easy visualization studies via IVIS live animal fluorescence imaging. For enhanced spatial resolution of AF700-CD40 within the tumor, we used 3D fluorescence tomography via IVIS (Figure S1B, Supporting Information). We focused on the tumor and peritumoral abdominal compartment for increased imaging efficiency. In a pilot study, we performed biodistribution analysis of AF700-CD40 over 7 days, comparing NDES-mediated sustained release to systemic delivery and bolus direct intratumoral injection (**Figure 2**A). Specifically, AF700-CD40 was delivered either via NDES with 20 nm membrane, a single intraperitoneal (IP) administration of 100, or 50 μg through one bolus intratumoral (IT) injection. A single dosage was administered so that Ab internalization/uptake and recycling can be tracked.[22] Dosage of CD40 mAb for IP and IT were chosen based on literature reports.[37–39] Based on the release profile, NDES is estimated to sustainably deliver a total of ≈21.0 μg CD40 mAb over 7 days.

In the IP group, spread of AF700-CD40 was apparent throughout the abdominal region within 5 min (0.003 day) after injection, as well as at the 4 h (0.17 day) timepoint (Figure 2A). Intratumoral accumulation was observed by day 4 after IP administration, with traces of fluorescent signal surrounding the tumor. Fluorescent signal was minimally visible in the IP-treated tumors by the end of the 7-day study, indicative of antibody clearance. As for the IT group, strong fluorescent signal was detected in the tumor immediately after injection (Figure 2A). However, AF700-CD40 gradually diffused out from the tumor over the course of the study, suggestive of rapid clearance. In contrast, the NDES group exhibited weak fluorescent signal in the tumor 5 min after intratumoral NDES implantation (Figure 2A). Within 4 h of intratumoral implantation, fluorescent signal of AF700-CD40 accumulated and was sustained throughout the study, attributable to constant release from the NDES. Analysis of the fluorescent signal intensity of the tumor over time showed the declining trend of both IP and IT groups, whereas sustained signal was evident in the NDES group after 4 h (Figure 2A).

At the end of the 7-day study, to further dissect drug biodistribution, we evaluated the tumors via ex vivo imaging for analysis unconfounded by skin, fur, or surrounding organs. Consistent with the in vivo imaging results, ex vivo radiance analysis of the tumors demonstrated high AF700-CD40 in the NDES group compared to IP and IT administration (Figure 2B). AF700 CD40 largely cleared out from the tumor in both IP and IT groups by day 7. Despite receving a higher dosage of AF700-CD40, the IP group had substantially lower radiance compared to IT and NDES groups, further suggestive of subpar drug localization to the tumor (Figure 2B). This is indicative of the advantage of sustained release via the NDES, whereby the need for redosing could be avoided. To evaluate systemic drug exposure, we assessed the liver for AF700-CD40 distribution (Figure 2B). The liver is a highly perfused and vascularized tissue and one of the primary sites of drug clearance.[40,41] As such, high concentration of systemically administered antibodies are typically observed in the liver.[41] Ex vivo imaging demonstrated AF700-CD40 exposure in the liver of the IP group, whereas there was no detectable signal either IT or NDES groups (Figure 2B). This result alludes to possible toxicity due to drug accumulation in the liver.

2.3. Reduction in Systemic Exposure with Intratumoral Administration

Because of the prevalence of liver accumulation in the pilot study, we sought to gain a more comprehensive view of systemic drug exposure over an extended duration. To investigate this, we performed a biodistribution study of AF700-CD40 in 4T1 tumor-bearing mice over 14 days. AF700-CD40 administration groups mirrored the pilot study, with the exception that 250 nm membrane was used in NDES group. The rationale for increasing nanochannel size was to enhance signal detection over the longer

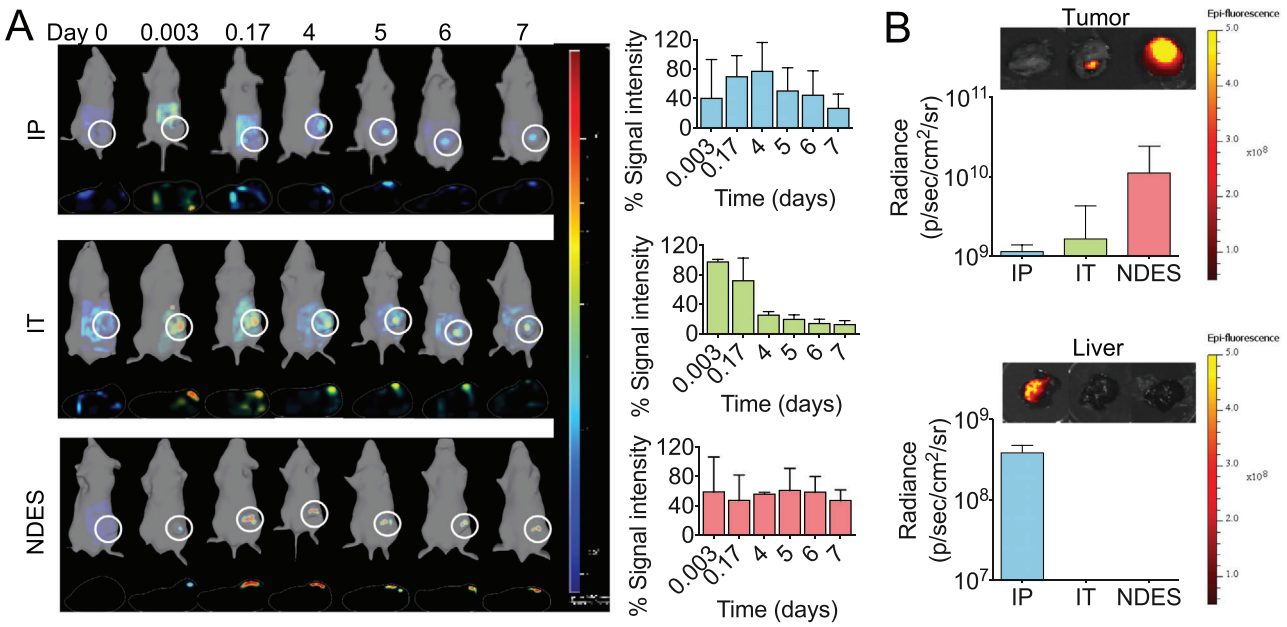

Figure 2. Sustained intratumoral distribution of AF700-CD40 via NDES in a 7-day study. A) Representative 3D renderings of IVIS fluorescence tomography images showing AF700-CD40 distribution in intraperitoneal (IP), intratumoral (IT) or NDES-treated 4T1 mice over 7 days. Tumors of 4T1 mice were treated with either 100 μg via IP administration ($n = 3$), 50 μg through bolus IT injection ($n = 3$), or implanted with AF700-CD40-filled NDES ($n = 3$, when tumor volume reached ≈100 mm^3. Fluorescence IVIS imaging was performed at 0.003 (5 min), 0.17 (4 h), and 4, 5, 6, and 7 days after AF700-CD40 administration. White circle denotes tumor. Fluorescent signal is represented in color. Pictured scale bars indicate strength of signal from low (blue) to high (red). Coronal (top panel) and transaxial (bottom panel) views are depicted. Bar graph depicts quantification of fluorescence signal intensity measured in the tumor from in vivo imaging, where % signal intensity in each graph is normalized to the highest signal within each group. B) Ex vivo fluorescence imaging analysis of the tumor and liver 7 days after AF700-CD40 administration. Bar graphs depict radiance signal measured (p sec^{-1} cm^{-2} sr^{-1}). Each data point represents mean ± STD.

study duration. In this arm of the experiment, we focused on antibody biodistribution across tissues as well as circulatory exposure.

We performed immunofluorescence imaging of histological tumor sections to visualize and quantify drug distribution within the tissue. We selected tumors from day 4 as an intermediate time point to allow for comparison of drug distribution prior to tumor clearance. 3D reconstruction of the sections showed diffuse dispersion of AF700-CD40 throughout the NDES-treated tumor, in contrary to lower signal in the IP and IT groups (**Figure 3**A). Signal quantification confirmed that the NDES group had significantly higher percentage of AF700-CD40 per tumor volume (1.38 ± 0.30%), compared to IP (0.18 ± 0.22%; $p < 0.02$) and IT (0.49 ± 0.30%; $p < 0.02$) groups (Figure 3B).

To evaluate drug dissemination, we examined relevant sites of antibody biodistribution, namely the liver, spleen, and lung[41] via ex vivo IVIS fluorescence imaging. In the IP group, fluorescence IVIS analysis revealed widespread dissemination of AF700-CD40 to the liver, spleen, and lung, specifically on days 1 and 4 after administration (**Figure 4**). As antibodies are primarily absorbed through the lymphatics,[40] we posit that substantial drug accumulation was observed in these organs due to their role in the lymphatic system. Of the examined organs, the lungs demonstrated the strongest drug accumulation within 1 day of IP administration. This is possibly attributable to rapid egress from the peritoneal space into the pleural cavity via lymphatic drainage.[42] As for the local administration groups, IT, and NDES, the nominal signal detected were considered negligible (Figure 4). These

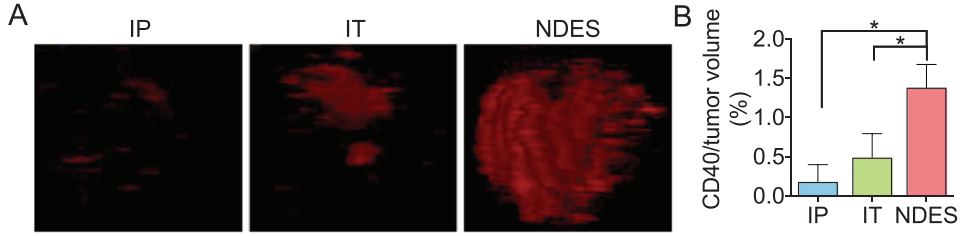

Figure 3. Visualization of AF700-CD40 distribution in the tumor via immunofluorescence imaging. A) Reconstructed confocal images of the tumor. B) Percentage AF700-CD40 per tumor volume in IP, IT, and NDES group. Each data point represents mean ± STD ($n = 3$). Statistical significance was determined via one-way ANOVA with Tukey test for multiple comparisons. *$p < 0.05$.

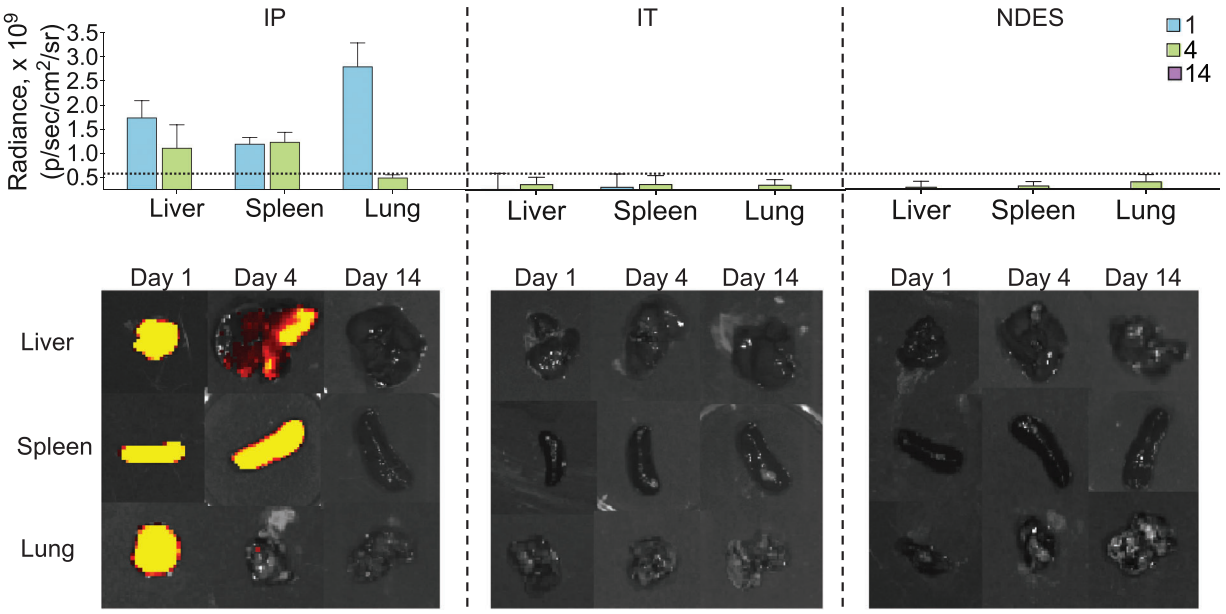

Figure 4. Biodistribution of AF700-CD40 across different organs over 14 days. Ex vivo fluorescence analysis of the liver, spleen, and lung were analyzed by measuring the radiance signal at the end of the 14-day study. Bar graphs depict radiance signal measured. Each data point represents mean ± STD (n = 6–7 per organ). Dotted horizontal line represents limit of detection.

organ analyses substantiated the systemic distribution of drug in the IP group, suggestive of the potential off-target organ toxicities.

2.4. Radiation Enhances Intratumoral Antibody Retention with NDES

Radiotherapy is increasingly investigated in combination with immunotherapy, with evidence of abscopal effects and improved response.[43–45] Thus it is important to understand the impact of radiation on drug biodistribution to the tumor. To investigate this, we compared AF700-CD40 tumor accumulation in radiated to non-radiated 4T1 mice over 14 days. Radiation was performed on a cohort of mice using 8 Gy consecutively over 3 days, followed by AF700-CD40 administration one day after the last irradiation. We chose this radiation dosage based on evidence of efficacy in the 4T1 tumor model in combination with immune checkpoint inhibitor.[46] The sequence of treatment was selected in accordance to the notion that radiation causes immunogenic cell death, which could augment efficacy of subsequent treatment with immunotherapy. Similar to the previous study, a single dose of immunotherapy was administered either via IP or IT injection, and compared to sustained release via NDES.

In vivo fluorescence IVIS imaging showed that in both IP and IT groups, AF700-CD40 cleared from the tumor over time regardless of radiation pre-treatment (**Figure 5**A). For the NDES group, enhanced intratumoral AF700-CD40 signal was visually detected in the radiation treatment cohort on days 4 and 14, compared to non-radiated mice. To further dissect this, we evaluated the tumors via ex vivo imaging 14 days after AF700-CD40 administration. As expected based on the in vivo imaging analysis, AF700-CD40 signal was undetectable in the IP group and minimally present in the IT group (Figure 5B). While IT group had minimal residual signal in the tumor, radiation did not affect drug retention. In contrast, ex vivo tumor imaging of the NDES group revealed augmented AF700-CD40 signal in the radiation treatment cohort, compared to non-radiated mice ($p < 0.01$; Figure 5B). It is plausible that enhanced tumor retention of AF700-CD40 occurred due to radiation-induced vascular and lymphatic damage, compromising clearance. On another note, we attribute the low fluorescence signal observed in the abdominal area to autofluorescence of chlorophyll-containing mouse chow. This is particularly apparent in the early time points (Day 0 and 0.003) in the NDES group. Nevertheless, we demonstrate increased AF700-CD40 in the NDES radiation treated cohort via ex vivo tumor imaging, which is intrinsically free of any potentially confounding effect of the skin, fur, and internal organs on the fluorescence signal.

Serum analysis showed a small degree of systemic exposure in the radiated NDES group (1.6 ± 2.0 μg mL^{-1}) upon study termination on day 14 (Figure 5C). We postulate that tumor saturating dose was reached due to cumulative effects of impaired tumor clearance and continuous release from the NDES, resulting in leakage into systemic circulation.[47] These results showed that when sustainably delivered via the NDES, pre-treatment with radiation enhances drug retention in the tumor.

3. Discussion

Spatiotemporal drug distribution in tumor tissue is a key factor in treatment response. When systemically delivered, mAb transport to the tumor is determined by numerous factors, including rate and extent of extravasation and permeability within tissue,

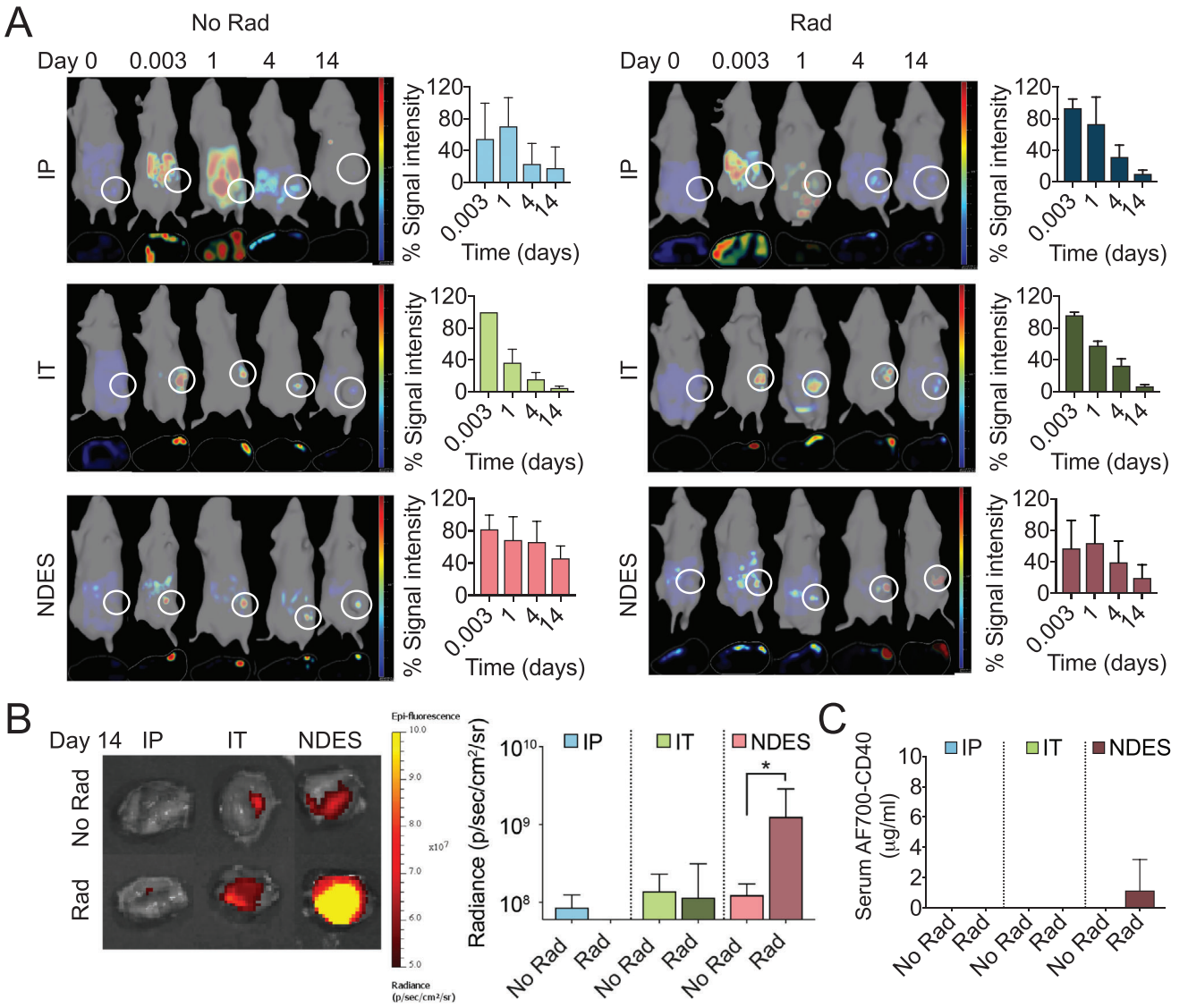

Figure 5. Fluorescent tomographic imaging comparison of radiation and route of administration of AF700-CD40 antibody over 14 days. A) Representative 3D renderings of IVIS fluorescence tomography images showing AF700-CD40 distribution in IP, IT, or NDES-treated 4T1 mice over 14 days, comparing radiation pre-treatment to non-irradiated cohort (n = 6–7 per group). In the radiated groups, tumors of 4T1 mice were irradiated with 8 Gy over three consecutive days, followed by AF700-CD40 administration either via IP (100 μg), direct bolus IT injection (50 μg), or NDES. Fluorescence IVIS imaging was performed at days 1, 4, and 14 days after AF700-CD40 administration. Tumors are denoted with white circles. Fluorescent signal is represented in color. Pictured scale bars indicate strength of signal from low (blue) to high (red). Bar graphs depict quantification of fluorescent signal, where % signal intensity in each graph is normalized to the highest signal within each group. Data shown are mean ± STD (n = 6–7 per group). B) Ex vivo fluorescence imaging analysis of the tumors 14 days after AF700-CD40 administration. Bar graphs depict radiance signal (p sec^{-1} cm^{-2} sr^{-1}). C) Serum AF700-CD40 levels of 4T1 mice administered via IP, IT, or NDES with or without radiation on day 14. Data shown are mean ± STD (n = 6–7 per group).

Ab binding to target, and elimination.[41,47] Moreover, FcRn and Fc interactions typically contributes to the distribution and clearance of mAb.[48] Specifically, recycling by Fc could affect plasma Ab clearance, which could impact tumor uptake. Drug transport can be further hindered by increased tumor interstitial fluid pressure and dense fibrotic tumor stroma, which can slow or impede penetration of therapeutic molecules.[49] As such, only <0.1% of systemically delivered Ab reaches target antigens within a solid tumor,[50] while widespread dissemination causes off-target adverse events. To overcome the tumor penetration barrier, intratumoral immunotherapy administration either via direct bolus injection or local controlled release technologies have emerged as appealing approaches. With the emergence of alternative routes of mAb administration, it is thus important to gain insights into their impact on biodistribution.

Here we demonstrate that sustained intratumoral administration via the NDES presents a viable method of surmounting the challenges of transport barriers and systemic exposure. We show that NDES achieves increased drug bioavailability in the tumor, as compared to IP or direct IT injection (Figure 2).

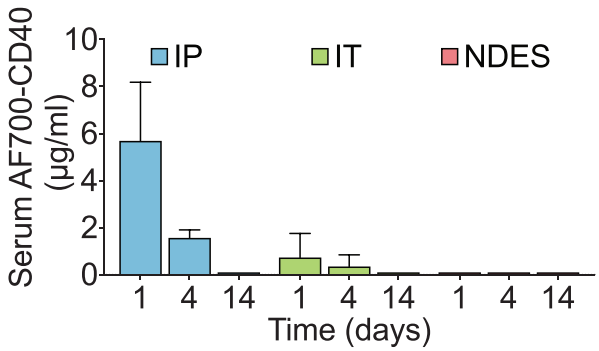

Figure 6. Serum AF700-CD40 levels of 4T1 mice administered over 14 days. ELISA analysis of serum drug levels of 4T1 mice administered with AF700-CD40 via IP, IT or NDES on days 1, 4, and 14. Each data point represents mean ± STD (n = 6–7 per timepoint).

This is particularly relevant in the context of CD40 mAb. In the clinic, systemically delivered CD40 mAb rarely reaches optimal therapeutic dose because of dose-limiting toxicities.[14] A recent approach to administer CD40 mAb (ADC-1013) directly into the tumor via IT injection encountered issues of toxicities similar to that of systemic delivery.[23] Specifically, ACD-1013 was detected in the serum immediately after IT injection, with concomitant increase in inflammatory cytokines. In our study, we demonstrate that while direct IT injection initially reaches high levels in the tumor, rapid seepage into systemic circulation occurred within a day of administration, albeit 8.1-fold lower than IP administration (**Figure 6**). This underscores the difficulty in maintaining local bioavailability with bolus direct IT injection. Clearance or leakage from the tumor is dependent on numerous factors, including drug metabolism locally,[47] tumor volume or degree of ulceration, necrosis, perfusion, and vascularization.[51–54] Further adding to the challenge of bolus IT injection is intratumoral pressure and tissue resistance, back leakage from injection canal, as well as injection position, volume, pressure, and technique.[55] In a phase I study of intratumoral interleukin-12 (IL-12) administration, plasma levels were detected within 30 min after injection, indicative of rapid leakage.[51] Compared to bolus intratumoral injections, the NDES releases drug in a slow, sustained manner via molecular concentration-driven diffusion. As such, in contrast to IT injections, with NDES administration no excess liquid is introduced in the tumor. Thus, we posit that drug clearance from the tumor occurs through a different and considerably slower mechanism than bolus injections. Although there has yet to be a clinical therapeutic standard for intratumoral immunotherapy dosage, CD40 mAb dosing ranged from 22.5 μg kg^{-1} up to 400 μg kg^{-1} in a recent trial.[23] The NDES can be tailored to achieve this dosing range through altering the size of the nanochannels or drug reservoir, as well as increasing quantity of implanted devices per tumor.

As previously shown,[56] compared to polymer-based drug-eluting systems, which have advantages of biodegradability or triggered delivery, the NDES does not have challenges of burst and decay release profiles, terminal dose-dumping, or require drug-specific formulation. Locally injectable drug-eluting platforms that rely on physiological enzymes or chemical stimuli for triggered release could potentially be impacted by the microenvironment, affecting dosing consistency.[57,58] In situ forming implants could pose concerns of drug release variability due to non-uniform geometry and shape reproducibility.[59–61] The NDES offers sustained release in a drug- and tissue- agnostic manner.

Composed of biocompatible, implantable materials, the NDES intended for long term intratumoral implantation. We have validated the tolerability of the material components of the NDES, as well as long term sustained drug release in numerous studies using small and animal models.[35,62–64] In the context of cancer treatment, while our current study is performed over 14 days, intratumoral implantation could be extended dependent on individual need. For example, in the case of neoadjuvant immunotherapy,[65–67] the NDES could be retrieved during tumor resection after predetermined immune priming phase. For patients with unresectable tumors, permanent placement similar to brachytherapy seeds is a viable alternative. Given the clinical precedence of intratumoral implants including that of the Comparative In Vivo Oncology device (NCT03056599),[68] we do not foresee implementation challenges with the NDES.

In our biodistribution analysis, the liver, spleen, and lungs demonstrated the most noticeable CD40 mAb accumulation when delivered systemically. In a relevant study using a murine bladder carcinoma model, CD40 mAb was demonstrated to primarily localize to the liver and spleen regardless of systemic or peritumoral administration.[22]

The distribution of CD40 mAb revealed in our study most likely reflects the abundance of target antigen-expressing cells in these organs.[22] Because CD40 is ubiquitously expressed in normal tissues, these organs become large antigen sinks and limit distribution to the tumor.[22,69] Thus, a larger systemic dose is required to saturate non-tumor tissue before reaching desirable therapeutic level in the tumor. As a result of the increased systemic exposure to immunotherapeutic Ab, accumulation occurs in off target organs, leading to various treatment-limiting toxicities.[7,70,71] The issue of antigen sinks in non-tumor tissue is not isolated to CD40; in fact, other immunotherapeutic targets encounter similar challenges, which impact efficacy as well as induce toxicities.[72–76] Of relevance, our results provide a possible explanation to the pronounced hepatotoxicity observed in the IP group compared to the NDES cohort in our previous study of CD40 efficacy in the 4T1 model.[27] Here we demonstrate that sustained release via the NDES minimizes systemic dissemination by avoiding distribution to non-tumor antigen sinks. Importantly, despite constant release from the NDES over 14 days, concomitant accumulation in organs were not detected. This suggests that with low dose slow release, biological clearance rate was sufficient to prevent significant systemic leakage.

Radiotherapy is implicated in influencing drug pharmacokinetics, leading to changes in treatment response or adverse effects.[77–79] A significant finding in our study is the effect of radiation pre-treatment on enhancing tumor retention, albeit only in the NDES group. We attribute this finding to radiation-induced vascular changes, resulting in impaired tumor clearance. However, this postulation needs to be validated in more extensive detailed investigations. Radiation is thought to impact vascular permeability, though inconsistencies persist across various preclinical studies.[80] These discrepancies are attributable to numerous factors including variability in mouse models, hypofractionated or non-hypofractionated dosing, dosage and

dosing regimen, radiation machinery and lead shielding.[80] Further, another notable point is that the effect of radiation on vascular permeability is possibly time dependent and transient. Maximal tumor uptake of systemically delivered Ab is demonstrated to be achieved when administered within 24 h of radiation.[81,82] Thereafter, reduced tumor interstitial fluid transport compromises intratumoral distribution of therapeutic Ab.[79] That said, in contrary to the NDES group, we did not observe changes in tumor uptake in the IP or IT group with radiation pre-treatment. While we allude to possible enhanced retention with sustained intratumoral delivery, on the basis of the controversial effects of radiation in literature, more studies are needed prior to making a conclusive interpretation.

In this biodistribution study, we chose labeling of mAb via fluorophore instead of the traditionally used radioisotopes. Depending on the radioisotope used, isotopes could either escape or be retained in the cells after mAb degradation.[41] Thus, radioisotope labeling could confound mAb distribution studies.[41] The small size of Alexa Fluor fluorophore (1025.2 g mol^{-1}) allows for mAb labeling without significantly affecting its size, and transport properties. Here we used *N*-Hydroxysuccinimide (NHS) ester chemistry to conjugate Alexa Fluor 700 to primary amines on CD40 mAb. Efficacy in terms of tumor inhibition were not evaluated due to single dose administered, as opposed to therapeutic dosage involving repeated dosing. In a prior study, we demonstrated comparable efficacy of NDES to IP administration of CD40 mAb, albeit without toxicities.[27]

4. Conclusion

Overall, from a clinical standpoint, our findings supports further investigation into the use of intratumoral slow release platforms to maximize tumor bioavailability. In this context, therapeutic mAbs not limited to CD40, such as checkpoint inhibitors with dose-dependent toxicity[83] could stand to benefit from minimizing systemic exposure. Further, future investigations involving concomitant biodistribution and efficacy with therapeutic doses are warranted to validate potential for clinical application.

5. Experimental Section

Reagents: Agonistic anti-mouse CD40 monoclonal antibody (CD40 mAb, clone FGK4.5, cat. #BP0016) was purchased from BioXCell (Lebanon, NH).

Fluorescent Antibody Conjugation and Lyophilization: Stock solution of CD40 mAb was concentrated via centrifugation in centricon tubes (Millipore) with molecular weight cutoff of 30 kDa. Filtrants were diluted in 0.1 M $NaHCO_3$, concentrated to displace stock buffer and cooled in an ice bath. AlexaFluor 700 *N*-Hydroxysuccinimide (NHS) ester (Invitrogen) was dissolved in dimethyl sulfoxide (DMSO), added to the antibody filtrant and stirred at 4 °C overnight. One fluorophore was conjugated to each CD40 mAb. The reaction mixture was washed with PBS, concentrated with centricon tubes and filtered through a 0.2 µm nylon filter. The absorbance of the filtered solution was measured via UV-Vis spectrophotometry at 280 and 693 nm. The concentration was calculated via the following equation:

$$C_{AF700-CD40} = \frac{\left(A_{280,m} - A_{693,m} * \frac{A_{280,\ AF700}}{A_{693,AF700}}\right)}{A_{280,CD40Ab}}$$

where $C_{AF700\text{-}aCD40}$ is the concentration of fluorescent Alexa Fluor 700-conjugated CD40 mAb (AF700-CD40 mAb), $A_{280,\,m}$ and $A_{693,\,m}$ are the measured absorbances of the solution at 280 and 693 nm, respectively, $A_{280,AF700}/A_{693,AF700}$ is the ratio of absorbances at 280 and 693 nm of unbound Alexa Fluor 700, and $A_{280,CD40Ab}$ is the absorbance at 280 nm of a 1 mg mL^{-1} solution of CD40 mAb. To stabilize the antibody for lyophilization, the antibody was combined with trehalose dehydrate at approximately 43% by mass, frozen at −80 °C, and lyophilized for 48 h in a standing lyophilizer (LabConco) at −32 °C and 0.09 mBar.

Nanofluidic Drug-Eluting Seed Fabrication: Silicon nanofluidic membranes microfabricated using a refined sacrificial etching process[34,84] and imaged via scanning electron microscopy (SEM; Nova NanoSEM 230, FEI, Oregon, USA). Nanofluidic drug-eluting seed (NDES) devices were fabricated as previously described.[27,32] Briefly, 18G 316 stainless steel tubes measuring 3 mm in length and 1.1 mm in diameter were used as the drug reservoir. Nanofluidic silicon membranes containing 20 or 250 nm nanochannels were affixed onto one end of the drug reservoir using thermal epoxy (EpoTek #354-T). We loaded the radio-opaque reservoir with lyophilized AF700-CD40 and sealed the open extremity with silicone adhesive (MED3-4213, Nusil) for 2 h at room temperature. A thin layer of ultraviolet (UV) epoxy (EPOTEK 0G116-31) was applied over the silicone adhesive cap to strengthen the drug reservoir seal and cured under UV light for 5 min. Each NDES was weighed before and after drug loading to determine total loaded antibody content. After loading, devices were submerged in PBS under vacuum conditions for 20 min to allow internal air to escape from the reservoir and prime the NDES for release.

In Vitro Release Rate Analysis: In vitro release analysis was performed as previously described.[27] Briefly, NDES (20 or 250 nm) loaded with CD40 were submerged in 2 mL of 1× PBS sink solution. The sink solution was collected and replaced daily with fresh 1× PBS. Collected samples were analyzed for protein concentration via µBCA assay (Pierce) according to the manufacturer's protocol. Release rate of the NDES over 21 days was calculated by fitting the cumulative release with a polynomial curve using MATLAB. A first degree polynomial was used and the best fit determined using the least-squares method.

Cell Line: The 4T1 murine mammary carcinoma cell line was obtained from ATCC. Cells were tested for pathogens by real time polymerase chain reaction and were routinely verified to be mycoplasma negative. Cells were cultured in RPMI 1640 supplemented with 2.05 mM L-glutamine, 100 IU mL^{-1} penicillin, and 100 µg mL^{-1} streptomycin at 37 °C and 5% CO_2.

Animals: 6-7-week-old Balb/c mice were obtained from Taconic Biosciences (Rensselaer, New York). Mice were housed in the comparative medicine facility at Houston Methodist Research Institute (HMRI, Houston, TX). Mice were acclimated to their new environment and given ad libitum food and water with a 12-h day/night cycle. All experiments were conducted according to protocol reviewed by an independent Institutional Animal Care and Use Committee (IACUC) and in accordance with the National Institutes of Health Guide for the Care and Use of Laboratory Animals and Animal Welfare Act and the ARRIVE guideline.

Tumor Model: To establish the 4T1 orthotopic mouse model, low passage 4T1 cells were suspended in 100 µL of a 3:1 PBS:Matrigel (Corning) mixture and injected into the 4th left mammary fat pad. Tumors were measured three times weekly using a digital caliper. Length was defined as the longest dimension measured and width was defined as the greatest dimension perpendicular to the lengthwise axis. Tumor volume was calculated according to the formula, (length × $width^2$)/2. When tumors were approximately 75–125 mm^3, mice were randomly assigned to groups.

Antibody Administration: NDES filled with AF700-CD40 was intratumorally inserted via a trocar approach using sterile procedures as previously described.[27] Lyophilized AF700-CD40 was dissolved in 1× PBS to at a concentration of 1 mg mL^{-1}. Mice were then injected with either 100 µL intraperitoneally for a dose of 100 µg or 50 µL intratumorally for a dose of 50 µg per animal. Dosage for IP was selected based on literature as well as due to similarity in pharmacodynamic effect in mice as the maximum tolerated dose of CP-870893 (human CD40 mAb) in patients.[85,86] IT dosage was selected based on literature.[39,87]

Small Animal Radiotherapy Administration: Prior to irradiation, mice were anesthetized with inhaled isoflurane and intraperitoneal

dexmedetomidine (5 μg g^{-1} body weight). Mice were secured to a plexiglass backboard with laboratory tape in the right lateral decubitus position. To limit radiation to the tumor, we shielded the mice with a combination of a rigid exposed-flank shield (Precision X-ray Inc.) and a flexible layer of lead. Radiotherapy was delivered at a rate of 4.3 Gy min^{-1} via an RS 2000 small animal irradiator (Rad Source). Dexmedetomidine anesthesia was reversed with atipamezole after radiation treatment was complete. Radiation was delivered in 8 Gy doses on three consecutive days. The radiation dosage was chosen based on previous literature.[46]

In Vivo Fluorescent Tomographic Imaging: Mice were shaved on both dorsum and ventrum before baseline image acquisition. Mice were anesthetized with isoflurane and placed supine on the imaging stage. The FLIT method of the IVIS Spectrum (Perkin Elmer) was used and 7–10 transillumination points were chosen over the tumor and abdominal region of the mice. For Alexa Fluor 700 detection, we used an excitation wavelength of 675 nm and an emission wavelength filter of 720 nm. Mice were imaged over a period of up to 14 days and the Living Image Software (Perkin Elmer) was used to acquire images and create 3D reconstructions. One mouse from the IP group in the pilot 7 day experiment died during the study. We analyzed the images in the Living Image Software by drawing a region of interest (ROI) around the tumor and measuring the fluorescent signal in radiance (p sec^{-1} cm^{-2} sr^{-1}). To better represent the trend in signal over time for each treatment, fluorescent signal intensity was plotted as "% signal intensity"; the animal with the highest signal intensity was considered 100%, by which normalization was performed for the signal intensities of the remaining mice within the group.[88]

Tissue Collection: Mice were sacrificed by CO_2 asphyxiation followed by cervical dislocation in accordance with institutional IACUC guidelines. Tumor, liver, spleen, and lungs, were collected. Blood was collected via cardiac puncture and transferred to serum separation tubes (BD). After centrifugation at 3500 × *g* for 4 min, serum was collected and stored at −80 °C.

Ex Vivo Organ Fluorescence Imaging Analysis: Organs were arranged on petri dishes. Ex vivo fluorescence imaging was performed using IVIS Spectrum (Xenogen/Perkin Elmer) at 675 nm excitation and 720 nm emission wavelength. Using the Living Image 4.5.2 software, regions of interest were indicated around each organ and the radiance values measured.

Frozen Tumor Tissue Preparation: Three tumors were randomly selected from each treatment group and sliced in thirds. Each tumor slice was embedded in Tissue-Tek OCT Compound in a plastic base mold. The molds were flash frozen in 2-methylbutane on dry ice for 30 s, wrapped in aluminum foil and stored at −80 °C until further processing.

Immunofluorescent Imaging of Tumors: Frozen tumor sections were cut into 30 μm slices using a cryostat with 230 μm between two adjacent slices. Every third slice was imaged via confocal microscopy and 3D reconstructed. For each sample, slices #1, 7, and 13 were selected for calculation of fluorescent distribution of Abs within the tumor using a custom-made MATLAB script which thresholds the images at 10% of the maximum intensity.[89,90] To minimize noise from tissue autofluorescence, a minimum signal level just below threshold for fluorescent Ab detection was set for each section. The area of distribution was calculated from each slice and multiplied by the slice thickness of 30 μm and summated across all images to obtain a total volume of distribution.

Anti-Rat IgG Enzyme-Linked Immunosorbent Assay: AF700-CD40 Ab was detected via an anti-rat IgG sandwich anti-rat IgG enzyme-linked immunosorbent assay (ELISA). 96-well Nunc Maxisorp plates (Thermo Fisher) were coated with anti-rat heavy chain antibody at 1.25 μg mL^{-1} (#MCA278, Bio-Rad Laboratories, Hercules, CA, USA) overnight at 4 °C. A standard curve was using AF700-CD40. The secondary antibody was an anti-rat kappa/lambda light chain antibody conjugated to horseradish peroxidase (#MCA1296P, Bio-Rad Laboratories). 1-Step UltraTMB (Thermo Fisher) was used as substrate and the colorimetric reaction as stopped with ELISA Stop Solution (Invitrogen). Plates were analyzed for absorbance at 450 nm in a UV–vis plate reader (BioTek Synergy H4).

Statistical Analysis: Statistical tests were performed in Graphpad Prism 7. Differences between groups were determined via student's *t*-test. $p < 0.05$ was considered significant.

Supporting Information

Supporting Information is available from the Wiley Online Library or from the author.

Acknowledgements

C.Y.X.C. and J.H. contributed equally to this manuscript. Funding support from NIH NCI U54 CA210181 (AG), Nancy Owens Breast Cancer Foundation (AG) and Golfers Against Cancer (AG). AG and research group received additional support through the Frank J. and Jean Raymond Centennial Chair Endowment. The authors thank Matthew Vasquez of the Houston Methodist ACTM core for support with confocal imaging, and Jianhua "James" Gu for SEM imaging. The authors thank Xukui Wang of the preclinical imaging core for assistance with the IVIS Spectrum analysis and Dr. Ramiro Pino for his support with dosimetry and shielding. The authors appreciate the help of Dr. Antons Sizovs with fluorophore labeling.

Conflict of Interest

The authors declare no conflict of interest.

Keywords

biodistribution, cancer immunotherapy, controlled release, intratumoral drug delivery, nanofluidics

Received: March 20, 2020
Revised: June 9, 2020
Published online:

[1] A. I. Minchinton, I. F. Tannock, *Nat. Rev. Cancer* **2006**, *6*, 583.
[2] F. Bensch, E. L. van der Veen, M. N. Lub-de Hooge, A. Jorritsma-Smit, R. Boellaard, I. C. Kok, S. F. Oosting, C. P. Schroder, T. J. N. Hiltermann, A. J. van der Wekken, H. J. M. Groen, T. C. Kwee, S. G. Elias, J. A. Gietema, S. S. Bohorquez, A. de Crespigny, S. P. Williams, C. Mancao, A. H. Brouwers, B. M. Fine, E. G. E. de Vries, *Nat. Med.* **2018**, *24*, 1852.
[3] I. H. Bartelink, E. F. Jones, S. K. Shahidi-Latham, P. R. E. Lee, Y. Zheng, P. Vicini, L. van 't Veer, D. Wolf, A. Iagaru, D. L. Kroetz, B. Prideaux, C. Cilliers, G. M. Thurber, Z. Wimana, G. Gebhart, *Clin. Pharmacol. Ther.* **2019**, *106*, 148.
[4] P. G. Baverel, V. F. S. Dubois, C. Y. Jin, Y. Zheng, X. Song, X. Jin, P. Mukhopadhyay, A. Gupta, P. A. Dennis, Y. Ben, P. Vicini, L. Roskos, R. Narwal, *Clin. Pharmacol. Ther.* **2018**, *103*, 631.
[5] C. Liu, J. Yu, H. Li, J. Liu, Y. Xu, P. Song, Q. Liu, H. Zhao, J. Xu, V. E. Maher, B. P. Booth, G. Kim, A. Rahman, Y. Wang, *Clin. Pharmacol. Ther.* **2017**, *101*, 657.
[6] A. N. Shoushtari, C. F. Friedman, P. Navid-Azarbaijani, M. A. Postow, M. K. Callahan, P. Momtaz, K. S. Panageas, J. D. Wolchok, P. B. Chapman, *JAMA Oncol.* **2018**, *4*, 98.
[7] A. Josefsson, J. R. Nedrow, S. Park, S. R. Banerjee, A. Rittenbach, F. Jammes, B. Tsui, G. Sgouros, *Cancer Res.* **2016**, *76*, 472.
[8] C. G. England, E. B. Ehlerding, R. Hernandez, B. T. Rekoske, S. A. Graves, H. Sun, G. Liu, D. G. McNeel, T. E. Barnhart, W. Cai, *J. Nucl. Med.* **2017**, *58*, 162.
[9] C. Y. X. Chua, J. S. Ho, S. Demaria, M. Ferrari, A. Grattoni, *Adv. Ther.* **2020**, *3*, 2000027.
[10] M. A. Aznar, N. Tinari, A. J. Rullán, A. R. Sánchez-Paulete, M. E. Rodriguez-Ruiz, I. Melero, *J. Immunol.* **2017**, *198*, 31.

[11] A. Marabelle, L. Tselikas, T. de Baere, R. Houot, *Ann. Oncol.* **2017**, *28*, xii33.
[12] S. B. Hassan, J. F. Sorensen, B. N. Olsen, A. E. Pedersen, *Immunopharmacol. Immunotoxicol.* **2014**, *36*, 96.
[13] R. H. Vonderheide, M. J. Glennie, *Clin. Cancer Res.* **2013**, *19*, 1035.
[14] D. A. Knorr, R. Dahan, J. V. Ravetch, *Proc. Natl. Acad. Sci. USA* **2018**, *115*, 11048.
[15] D. M. Richards, J. P. Sefrin, C. Gieffers, O. Hill, C. Merz, *Hum. Vaccines Immunother.* **2020**, *16*, 377.
[16] R. H. Vonderheide, K. T. Flaherty, M. Khalil, M. S. Stumacher, D. L. Bajor, N. A. Hutnick, P. Sullivan, J. J. Mahany, M. Gallagher, A. Kramer, S. J. Green, P. J. O'Dwyer, K. L. Running, R. D. Huhn, S. J. Antonia, *J. Clin. Oncol.* **2007**, *25*, 876.
[17] D. L. Bajor, R. Mick, M. J. Riese, A. C. Huang, B. Sullivan, L. P. Richman, D. A. Torigian, S. M. George, E. Stelekati, F. Chen, J. J. Melenhorst, S. F. Lacey, X. Xu, E. J. Wherry, T. C. Gangadhar, R. K. Amaravadi, L. M. Schuchter, R. H. Vonderheide, *Oncoimmunology* **2018**, *7*, e1468956.
[18] J. Ruter, S. J. Antonia, H. A. Burris, R. D. Huhn, R. H. Vonderheide, *Cancer Biol. Ther.* **2010**, *10*, 983.
[19] M. F. Fransen, M. Sluijter, H. Morreau, R. Arens, C. J. Melief, *Clin. Cancer Res.* **2011**, *17*, 2270.
[20] S. M. Mangsbo, S. Broos, E. Fletcher, N. Veitonmaki, C. Furebring, E. Dahlen, P. Norlen, M. Lindstedt, T. H. Totterman, P. Ellmark, *Clin. Cancer Res.* **2015**, *21*, 1115.
[21] S. Rahimian, M. F. Fransen, J. W. Kleinovink, M. Amidi, F. Ossendorp, W. E. Hennink, *Biomaterials* **2015**, *61*, 33.
[22] L. C. Sandin, A. Orlova, E. Gustafsson, P. Ellmark, V. Tolmachev, T. H. Totterman, S. M. Mangsbo, *Cancer Immunol. Res.* **2014**, *2*, 80.
[23] S. M. M. Irenaeus, D. Nielsen, P. Ellmark, J. Yachnin, A. Deronic, A. Nilsson, P. Norlen, N. Veitonmaki, C. S. Wennersten, G. J. Ullenhag, *Int. J. Cancer* **2019**, *145*, 1189.
[24] L. Milling, Y. Zhang, D. J. Irvine, *Adv. Drug Deliv. Rev.* **2017**, *114*, 79.
[25] J. B. Wolinsky, Y. L. Colson, M. W. Grinstaff, *J. Controlled Release* **2012**, *159*, 14.
[26] M. F. Fransen, R. A. Cordfunke, M. Sluijter, M. J. van Steenbergen, J. W. Drijfhout, F. Ossendorp, W. E. Hennink, C. J. Melief, *Vaccine* **2014**, *32*, 1654.
[27] C. Y. X. Chua, P. Jain, A. Susnjar, J. Rhudy, M. Folci, A. Ballerini, A. Gilbert, S. Singh, G. Bruno, C. S. Filgueira, C. Yee, E. B. Butler, A. Grattoni, *J. Controlled Release* **2018**, *285*, 23.
[28] S. Demaria, E. B. Golden, S. C. Formenti, *JAMA Oncol.* **2015**, *1*, 1325.
[29] A. J. Rech, H. Dada, J. J. Kotzin, J. Henao-Mejia, A. J. Minn, C. Twyman-Saint Victor, R. H. Vonderheide, *Cancer Res.* **2018**, *78*, 4282.
[30] S. Yasmin-Karim, P. T. Bruck, M. Moreau, S. Kunjachan, G. Z. Chen, R. Kumar, S. Grabow, S. K. Dougan, W. Ngwa, *Front. Immunol.* **2018**, *9*, 2030.
[31] I. Verbrugge, J. Hagekyriakou, L. L. Sharp, M. Galli, A. West, N. M. McLaughlin, H. Duret, H. Yagita, R. W. Johnstone, M. J. Smyth, N. M. Haynes, *Cancer Res.* **2012**, *72*, 3163.
[32] R. L. Hood, G. Bruno, P. Jain, J. Anderson, T. Wolfe, C. Quini, J. Schmulen, X. C. Li, E. B. Butler, S. Krishnan, A. Grattoni, *J. Biomed. Nanotechnol.* **2016**, *12*, 1907.
[33] D. Fine, A. Grattoni, S. Hosali, A. Ziemys, E. De Rosa, J. Gill, R. Medema, L. Hudson, M. Kojic, M. Milosevic, L. Brousseau Iii, R. Goodall, M. Ferrari, X. Liu, *Lab Chip* **2010**, *10*, 3074.
[34] G. Bruno, N. Di Trani, R. L. Hood, E. Zabre, C. S. Filgueira, G. Canavese, P. Jain, Z. Smith, D. Demarchi, S. Hosali, A. Pimpinelli, M. Ferrari, A. Grattoni, *Nat. Commun.* **2018**, *9*, 1682.
[35] S. Ferrati, D. Fine, J. You, E. De Rosa, L. Hudson, E. Zabre, S. Hosali, L. Zhang, C. Hickman, S. Sunder Bansal, A. M. Cordero-Reyes, T. Geninatti, J. Sih, R. Goodall, G. Palapattu, M. Kloc, R. M. Ghobrial, M. Ferrari, A. Grattoni, *J. Control Release* **2013**, *172*, 1011.
[36] N. Di Trani, A. Pimpinelli, A. Grattoni, *ACS Appl. Mater. Interfaces* **2020**, *12*, 12246.
[37] S. H. Ahn, J. Y. Choi, S. D. Kim, S. J. Park, H. Kim, *Oncol. Lett.* **2019**, *18*, 5889.
[38] T. Shoji, R. Saito, M. Chonan, I. Shibahara, A. Sato, M. Kanamori, Y. Sonoda, T. Kondo, N. Ishii, T. Tominaga, *Neuro Oncol.* **2016**, *18*, 1120.
[39] M. Singh, C. Vianden, M. J. Cantwell, Z. Dai, Z. Xiao, M. Sharma, H. Khong, A. R. Jaiswal, F. Faak, Y. Hailemichael, L. M. E. Janssen, U. Bharadwaj, M. A. Curran, A. Diab, R. L. Bassett, D. J. Tweardy, P. Hwu, W. W. Overwijk, *Nat. Commun.* **2017**, *8*, 1447.
[40] L. Liu, *Protein Cell* **2018**, *9*, 15.
[41] D. K. Shah, A. M. Betts, *mAbs* **2013**, *5*, 297.
[42] J. S. Barrett, J. G. Wagner, S. J. Fisher, R. L. Wahl, *Cancer Res.* **1991**, *51*, 3434.
[43] W. Ngwa, O. C. Irabor, J. D. Schoenfeld, J. Hesser, S. Demaria, S. C. Formenti, *Nat. Rev. Cancer* **2018**, *18*, 313.
[44] S. Demaria, C. N. Coleman, S. C. Formenti, *Trends Cancer* **2016**, *2*, 286.
[45] S. C. Formenti, N. P. Rudqvist, E. Golden, B. Cooper, E. Wennerberg, C. Lhuillier, C. Vanpouille-Box, K. Friedman, L. Ferrari de Andrade, K. W. Wucherpfennig, A. Heguy, N. Imai, S. Gnjatic, R. O. Emerson, X. K. Zhou, T. Zhang, A. Chachoua, S. Demaria, *Nat. Med.* **2018**, *24*, 1845.
[46] M. Z. Dewan, A. E. Galloway, N. Kawashima, J. K. Dewyngaert, J. S. Babb, S. C. Formenti, S. Demaria, *Clin. Cancer Res.* **2009**, *15*, 5379.
[47] G. M. Thurber, R. Weissleder, *PLoS One* **2011**, *6*, e24696.
[48] G. M. Thurber, M. M. Schmidt, K. D. Wittrup, *Adv. Drug. Deliv. Rev.* **2008**, *60*, 1421.
[49] A. I. Minchinton, I. F. Tannock, *Nat. Rev. Cancer* **2006**, *6*, 583.
[50] J. Christiansen, A. K. Rajasekaran, *Mol. Cancer Ther.* **2004**, *3*, 1493.
[51] C. M. Van Herpen, R. Huijbens, M. Looman, J. De Vries, H. Marres, J. Van De Ven, R. Hermsen, G. J. Adema, P. H. De Mulder, *Clin. Cancer Res.* **2003**, *9*, 2950.
[52] C. M. van Herpen, M. Looman, M. Zonneveld, N. Scharenborg, P. C. de Wilde, L. van de Locht, M. A. Merkx, G. J. Adema, P. H. de Mulder, *Clin. Cancer Res.* **2004**, *10*, 2626.
[53] B. Weide, E. Derhovanessian, A. Pflugfelder, T. K. Eigentler, P. Radny, H. Zelba, C. Pfohler, G. Pawelec, C. Garbe, *Cancer* **2010**, *116*, 4139.
[54] A. Saleem, P. M. Price, *Clin. Cancer Res.* **2008**, *14*, 8184.
[55] R. C. Bakker, M. Lam, S. A. van Nimwegen, A. Rosenberg, R. J. J. van Es, J. F. W. Nijsen, *J. Radiat. Oncol.* **2017**, *6*, 323.
[56] S. Ferrati, E. Nicolov, E. Zabre, T. Geninatti, B. A. Shirkey, L. Hudson, S. Hosali, M. Crawley, M. Khera, G. Palapattu, A. Grattoni, *J. Sex Med.* **2015**, *12*, 1375.
[57] S. Yu, C. Wang, J. Yu, J. Wang, Y. Lu, Y. Zhang, X. Zhang, Q. Hu, W. Sun, C. He, X. Chen, Z. Gu, *Adv. Mater.* **2018**, *30*, 1801527.
[58] R. S. Riley, C. H. June, R. Langer, M. J. Mitchell, *Nat. Rev. Drug. Discov.* **2019**, *18*, 175.
[59] M. Parent, C. Nouvel, M. Koerber, A. Sapin, P. Maincent, A. Boudier, *J. Control Release* **2013**, *172*, 292.
[60] M. Nishikawa, K. Ogawa, Y. Umeki, K. Mohri, Y. Kawasaki, H. Watanabe, N. Takahashi, E. Kusuki, R. Takahashi, Y. Takahashi, Y. Takakura, *J. Control Release* **2014**, *180*, 25.
[61] C. Hernandez, A. A. Exner, *Ther. Deliv.* **2017**, *8*, 479.
[62] C. Y. X. Chua, P. Jain, A. Ballerini, G. Bruno, R. L. Hood, M. Gupte, S. Gao, N. Di Trani, A. Susnjar, K. Shelton, L. R. Bushman, M. Folci, C. S. Filgueira, M. A. Marzinke, P. L. Anderson, M. Hu, P. Nehete, R. C. Arduino, J. K. Sastry, A. Grattoni, *J. Control Release* **2018**, *286*, 315.
[63] C. S. Filgueira, G. Bruno, Z. W. Smith, C. Y. X. Chua, A. Ballerini, M. Folci, A. L. Gilbert, P. Jain, J. K. Sastry, P. N. Nehete, K. A. Shelton, L. R. Hill, A. Ali, K. A. Youker, A. Grattoni, *Biomed. Microdevices* **2018**, *20*, 49.

[64] F. P. Pons-Faudoa, A. Sizovs, N. Di Trani, J. Paez-Mayorga, G. Bruno, J. Rhudy, M. Manohar, K. Gwenden, C. Martini, C. Y. X. Chua, G. Varchi, M. A. Marzinke, A. Grattoni, *J. Control Release* **2019**, *306*, 89.
[65] C. U. Blank, E. A. Rozeman, L. F. Fanchi, K. Sikorska, B. van de Wiel, P. Kvistborg, O. Krijgsman, M. van den Braber, D. Philips, A. Broeks, J. V. van Thienen, H. A. Mallo, S. Adriaansz, S. Ter Meulen, L. M. Pronk, L. G. Grijpink-Ongering, A. Bruining, R. M. Gittelman, S. Warren, H. van Tinteren, D. S. Peeper, J. Haanen, A. C. J. van Akkooi, T. N. Schumacher, *Nat. Med.* **2018**, *24*, 1655.
[66] E. Z. Keung, E. U. Ukponmwan, A. P. Cogdill, J. A. Wargo, *Ann. Surg. Oncol.* **2018**, *25*, 1814.
[67] E. A. Rozeman, A. M. Menzies, A. C. J. van Akkooi, C. Adhikari, C. Bierman, B. A. van de Wiel, R. A. Scolyer, O. Krijgsman, K. Sikorska, H. Eriksson, A. Broeks, J. V. van Thienen, A. D. Guminski, A. T. Acosta, S. Ter Meulen, A. M. Koenen, L. J. W. Bosch, K. Shannon, L. M. Pronk, M. Gonzalez, S. Ch'ng, L. G. Grijpink-Ongering, J. Stretch, S. Heijmink, H. van Tinteren, J. Haanen, O. E. Nieweg, W. M. C. Klop, C. L. Zuur, R. P. M. Saw, W. J. van Houdt, D. S. Peeper, A. J. Spillane, J. Hansson, T. N. Schumacher, G. V. Long, C. U. Blank, *Lancet Oncol.* **2019**, *20*, 948.
[68] R. A. Klinghoffer, S. B. Bahrami, B. A. Hatton, J. P. Frazier, A. Moreno-Gonzalez, A. D. Strand, W. S. Kerwin, J. R. Casalini, D. J. Thirstrup, S. You, S. M. Morris, K. L. Watts, M. Veiseh, M. O. Grenley, I. Tretyak, J. Dey, M. Carleton, E. Beirne, K. D. Pedro, S. H. Ditzler, E. J. Girard, T. L. Deckwerth, J. A. Bertout, K. A. Meleo, E. H. Filvaroff, R. Chopra, O. W. Press, J. M. Olson, *Sci. Transl. Med.* **2015**, *7*, 284ra258.
[69] R. H. Vonderheide, *Cancer Cell* **2018**, *33*, 563.
[70] Y. Zen, M. M. Yeh, *Mod. Pathol.* **2018**, *31*, 965.
[71] K. Zarrabi, S. Wu, *Oncology* **2018**, *94*, 259.
[72] E. Dheilly, V. Moine, L. Broyer, S. Salgado-Pires, Z. Johnson, A. Papaioannou, L. Cons, S. Calloud, S. Majocchi, R. Nelson, F. Rousseau, W. Ferlin, M. Kosco-Vilbois, N. Fischer, K. Masternak, *Mol. Ther.* **2017**, *25*, 523.
[73] J. R. Ingram, O. S. Blomberg, J. T. Sockolosky, L. Ali, F. I. Schmidt, N. Pishesha, C. Espinosa, S. K. Dougan, K. C. Garcia, H. L. Ploegh, M. Dougan, *Proc. Natl. Acad. Sci. USA* **2017**, *114*, 10184.
[74] K. Broos, Q. Lecocq, G. Raes, N. Devoogdt, M. Keyaerts, K. Breckpot, *Theranostics* **2018**, *8*, 3559.
[75] R. Deng, D. Bumbaca, C. V. Pastuskovas, C. A. Boswell, D. West, K. J. Cowan, H. Chiu, J. McBride, C. Johnson, Y. Xin, H. Koeppen, M. Leabman, S. Iyer, *mAbs* **2016**, *8*, 593.
[76] J. R. Nedrow, A. Josefsson, S. Park, S. Ranka, S. Roy, G. Sgouros, *J. Nucl. Med.* **2017**, *58*, 1560.
[77] Y. J. Chen, T. H. Tsai, L. Y. Wang, C. H. Hsieh, *Technol. Cancer Res. Treat.* **2017**, *16*, 705.
[78] A. W. Blackstock, L. Kwock, C. Branch, E. M. Zeman, J. E. Tepper, *Int. J. Radiat. Oncol. Biol. Phys.* **1996**, *36*, 641.
[79] C. A. Znati, M. Rosenstein, T. D. McKee, E. Brown, D. Turner, W. D. Bloomer, S. Watkins, R. K. Jain, Y. Boucher, *Clin. Cancer Res.* **2003**, *9*, 5508.
[80] I. Martinez-Zubiaurre, A. J. Chalmers, T. Hellevik, *Front. Immunol.* **2018**, *9*, 1679.
[81] H. Kalofonos, G. Rowlinson, A. A. Epenetos, *Cancer Res.* **1990**, *50*, 159.
[82] S. Ruan, J. A. O'Donoghue, S. M. Larson, R. D. Finn, A. Jungbluth, S. Welt, J. L. Humm, *J. Nucl. Med.* **2000**, *41*, 1905.
[83] A. Bertrand, M. Kostine, T. Barnetche, M. - E. Truchetet, T. Schaeverbeke, *BMC Med.* **2015**, *13*, 211.
[84] D. Fine, A. Grattoni, S. Hosali, A. Ziemys, E. De Rosa, J. Gill, R. Medema, L. Hudson, M. Kojic, M. Milosevic, L. Brousseau Iii, R. Goodall, M. Ferrari, X. Liu, *Lab Chip* **2010**, *10*, 3074.
[85] L. P. Richman, R. H. Vonderheide, *Cancer Immunol. Res.* **2014**, *2*, 19.
[86] G. L. Beatty, E. G. Chiorean, M. P. Fishman, B. Saboury, U. R. Teitelbaum, W. Sun, R. D. Huhn, W. Song, D. Li, L. L. Sharp, D. A. Torigian, P. J. O'Dwyer, R. H. Vonderheide, *Science* **2011**, *331*, 1612.
[87] J. Ishihara, A. Ishihara, L. Potin, P. Hosseinchi, K. Fukunaga, M. Damo, T. F. Gajewski, M. A. Swartz, J. A. Hubbell, *Mol. Cancer Ther.* **2018**, *17*, 2399.
[88] C. G. Park, C. A. Hartl, D. Schmid, E. M. Carmona, H. J. Kim, M. S. Goldberg, *Sci. Transl. Med.* **2018**, *10*.
[89] C. Zhang, P. Mastorakos, M. Sobral, S. Berry, E. Song, E. Nance, C. G. Eberhart, J. Hanes, J. S. Suk, *J. Control Release* **2017**, *267*, 232.
[90] C. Zhang, E. A. Nance, P. Mastorakos, J. Chisholm, S. Berry, C. Eberhart, B. Tyler, H. Brem, J. S. Suk, J. Hanes, *J. Control Release* **2017**, *263*, 112.